

Abstract

There are many contributing factors which determine the micro- and macrophysical properties of clouds, including atmospheric structure, dominant meteorological conditions, and aerosol concentration, all of which may be coupled to one another. In the quest to determine aerosol effects on clouds, these potential relationships must be understood, as changes in atmospheric conditions due to aerosol may change the expected magnitude of indirect effects by altering cloud properties in unexpected ways. Here we describe several observed correlations between aerosol conditions and cloud and atmospheric properties in the Indian Ocean winter monsoon season.

In the CARDEX (Cloud, Aerosol, Radiative forcing, Dynamics EXperiment) field campaign conducted in February and March 2012 in the northern Indian Ocean, continuous measurements of atmospheric precipitable water vapor and the liquid water path (LWP) of trade cumulus clouds were made, concurrent with measurements of water vapor flux, cloud and aerosol vertical profiles, meteorological data, and surface and total-column aerosol. Here we present evidence of a positive correlation between aerosol and cloud LWP which becomes clear after the data are filtered to control for the natural meteorological variability in the region.

We then use the aircraft and ground observatory measurements to explore the mechanisms behind the observed aerosol–LWP correlation. We determine that increased boundary-layer humidity lowering the cloud base is responsible for the observed increase in cloud liquid water. Large-scale analysis indicates that high pollution cases originate with a highly-polluted boundary layer air mass approaching the observatory from a northwesterly direction. This polluted mass exhibits higher temperatures and humidity than the clean case, the former of which may be attributable to heating due to aerosol absorption of solar radiation over the subcontinent. While high temperature conditions dispersed along with the high-aerosol anomaly, the high humidity condition was observed to instead develop along with the polluted air mass. We then explore

Atmospheric aerosol effects in a trade cumulus regime

K. Pistone et al.

Title Page

Abstract

Introduction

Conclusions

References

Tables

Figures



Back

Close

Full Screen / Esc

Printer-friendly Version

Interactive Discussion



potential causal mechanisms of the observed correlations, though future research will be needed to more fully describe the aerosol–humidity relationship.

1 Introduction

The northern Indian Ocean is a region of great interest in aerosol studies, due to frequent episodes of polluted air arriving from the Indian subcontinent. The current study builds upon a long history of studies in the region, starting with the Indian Ocean Experiment (INDOEX) in 1998–1999 (Ramanathan et al., 2001). INDOEX, the result of collaboration between multiple international organizations led by Scripps Institution of Oceanography, made simultaneous multi-platform measurements in the Indian Ocean with the goal of observationally constraining direct and indirect effects of aerosols in the region, in particular the atmospheric heating and surface cooling caused by the presence of black carbon (BC) aerosols within the atmospheric column. The intensive field operations allowed scientists to, for the first time, quantify the direct radiative effects of absorbing aerosols originating in southeast Asia, and contrast the highly-polluted conditions north of the ITCZ with pristine Southern Hemisphere conditions (e.g. Heymsfield and McFarquhar, 2001). INDOEX would set the stage for later work in the region investigating the effects of absorbing aerosols within the atmospheric column.

The 2006 Maldives Autonomous unmanned aerial vehicle Campaign (MAC) investigated the role of absorbing aerosols in the Indian Ocean, and their effects on clouds, using lightweight unmanned aerial vehicles (UAVs) with miniaturized radiation, aerosol, and cloud instrumentation as payload (Ramanathan et al., 2007; Ramana et al., 2007; Corrigan et al., 2008; Roberts et al., 2008). The UAVs were flown stacked one on top of the other and, with their upward- and downward-looking instrumentation operating simultaneously, directly measured the amount of radiation absorbed within an aerosol layer (Ramanathan et al., 2007). CARDEX follows from these previous studies using UAVs and ground measurements, and for the first time incorporates flux measurements for a greater focus on dynamics and how aerosol may be influencing clouds.

Atmospheric aerosol effects in a trade cumulus regime

K. Pistone et al.

Title Page

Abstract

Introduction

Conclusions

References

Tables

Figures



Back

Close

Full Screen / Esc

Printer-friendly Version

Interactive Discussion



Atmospheric aerosol effects in a trade cumulus regime

K. Pistone et al.

Title Page

Abstract

Introduction

Conclusions

References

Tables

Figures



Back

Close

Full Screen / Esc

Printer-friendly Version

Interactive Discussion



Between 16 February and 30 March 2012, the Cloud, Aerosol, Radiative forcing, and Dynamics EXperiment (CARDEX) was conducted on Hanimaadhoo Island, Maldives (Fig. 1), led by scientists from Scripps Institution of Oceanography in San Diego, California and including collaborators from the Desert Research Institute in Reno, Nevada; Stockholm University in Stockholm, Sweden; Max Planck Institute for Chemistry in Mainz, Germany; and Argonne National Lab in Argonne, Illinois. The Maldives Climate Observatory at Hanimaadhoo (MCOH) has been making continuous measurements of aerosol, radiation, and meteorological parameters on Hanimaadhoo Island since October 2004 (Ramana and Ramanathan, 2006). During the CARDEX campaign, measurements from small aircraft were supplemented with the continuous ground measurements at MCOH, including additional instruments exclusive to the CARDEX period: a mini-micropulse lidar (MPL), to measure cloud base height, boundary layer height, and the altitude of elevated aerosol plumes; and a microwave radiometer (MWR), to measure total-column precipitable water vapor and cloud liquid water path. CARDEX was designed to observe the atmosphere at the end of the so-called dry season (winter monsoon), a time when atmospheric flow over the Maldives is predominantly from the highly-polluted Indian subcontinent with little wet removal due to rainfall. The atmospheric conditions in this season are heavily influenced by anthropogenic pollution, and thus the site, and this study, are valuable to a broader understanding of aerosol effects.

Here we present new observations of the dry season climatology of this trade cumulus regime, including cloud, aerosol, and meteorological properties, as observed during CARDEX. In Sect. 2, we describe two distinct categories of atmospheric properties, here termed “wet” and “dry” regimes, and explain the differing conditions resulting in each. In Sect. 3, we describe the aerosol–cloud correlations which were observed in CARDEX and use the systematic distinctions between low and high pollution cases to gain insight into the mechanisms governing the observed differences in cloud properties. We then offer brief speculation on some potential causal factors of the observed

correlations, including the role of aerosol in modifying atmospheric humidity and the potential implications for the understanding of aerosol effects on clouds.

Methods

In the following sections, unless otherwise stated, the aerosol conditions presented have been determined by the aerosol number concentration as measured by the condensation particle counter (CPC) instrument at MCOH (Fig. 2). Other aerosol metrics used are aerosol optical depth (AOD) as measured both by the MCOH AERONET sun photometer; satellite-based AOD from the MODIS instruments on board NASA's Terra and Aqua satellites; and black carbon (BC) concentration measured by an airborne or ground-based aethalometer.

The cloud liquid water path (LWP) given here is the average-peak value (the mean of all cloud retrievals within 100 g m^{-2} of the peak cloud value) for each cloud event (Fig. 3). This definition preserves the peak LWP as a characteristic of the cloud (Warner, 1955) while accounting for instrument noise and variability within the cloud. Further discussion of identification and processing of cloud "events" is given in Appendix A1.

Three unmanned aerial vehicles (UAVs) were flown during CARDEX. MAC4, MAC5, and MAC6 flew the aerosol-radiation, water vapor flux, and cloud microphysics payloads, respectively. A more detailed description of each payload may be found in Ramanathan et al. (2007); Ramana et al. (2007); Corrigan et al. (2008); Roberts et al. (2008); Thomas et al. (2012).

A complete description of the permanent MCOH instrumentation and data used in this paper has been given in Ramana and Ramanathan (2006). Additional information on the CARDEX-specific instrumentation used, including the lidar and the microwave radiometer, may be found in the Appendix A1.

Atmospheric aerosol effects in a trade cumulus regime

K. Pistone et al.

Title Page

Abstract

Introduction

Conclusions

References

Tables

Figures



Back

Close

Full Screen / Esc

Printer-friendly Version

Interactive Discussion



2 Atmospheric regime as indicated by total-column water vapor content

The high variability in total-column atmospheric water vapor observed during CARDEX (ranging from 20–60 kg m⁻², Fig. 2) allows one to categorize the observations as either “wet” (here defined as total-column PWV > 40 kg m⁻²; blue in Fig. 2) or “dry” (total-column PWV < 40 kg m⁻²; black in Fig. 2). This distinction allows insight into specific aspects of atmospheric structure in the region.

In this analysis, vapor conditions are identified primarily using the MWR total-column PWV, chosen for its high temporal resolution. Using the good agreement between the MWR and AERONET column PWV, the CARDEX flight days before MWR operations began on 6 March are additionally classified. Daily-averaged PWV conditions for the entire CARDEX period are given in Table 1, and classifications for each UAV flight are given in Table 2.

2.1 Observed distinctions between dry and wet atmospheric conditions

Table 3 shows the differences in observed MCOH surface parameters for wet vs. dry conditions on one-minute resolution. There are some prominent differences between the two populations: on average, dry cases correspond to higher wind speed in both north–south and east–west directions, as well as lower surface pressures; as may be expected, the surface humidity is also greater for wet cases, and wet days also exhibit greater variability in cloud LWP. Figures A1 and A2 illustrate the frequency distributions of parameters measured for wet vs. dry conditions. There were no significant differences in observed average aerosol amount (CPC number concentration or AERONET column AOD), cloud or boundary layer height, or surface fluxes between the two populations when considering the variability of the observations.

The vertical profiles from the MAC4 aircraft under wet (dark blue) and dry (cyan, black) conditions are shown in Fig. 4. It is first notable that in both categories, the UAV profiles indicate large variability in aerosol throughout the atmospheric column (i.e. both boundary layer aerosol and free troposphere aerosol), in terms of CPC number con-

Atmospheric aerosol effects in a trade cumulus regime

K. Pistone et al.

Title Page

Abstract

Introduction

Conclusions

References

Tables

Figures



Back

Close

Full Screen / Esc

Printer-friendly Version

Interactive Discussion



2.2 Large-scale contrasts between high and low water vapor conditions

In exploring the mechanisms which may contribute to this wet/dry distinction, we analyze air mass back trajectories as determined by the NOAA HYSPLIT model (Fig. 5). While there is large variability in lower-level flow for both wet and dry cases, there are consistent differences in the upper-level flow of each case. On extremely dry days (Fig. 5a), the back trajectories indicate that upper-level atmospheric flow originates over the Indian subcontinent, traveling in an anticyclonic motion before arriving at MCOH as northeasterlies. During the 7 day air mass history, the air was continuously descending to the 2–3 km range. In contrast, for high-PWV conditions (Fig. 5b), upper-level air masses are easterly, approaching from the Bay of Bengal and Indonesia, and the 2–3 km air over MCOH has ascended from the boundary layer to the free troposphere within 4 days of observation. These results are consistent with the aircraft measurement results: the primary distinction between wet and dry cases is in the upper-level air mass conditions: in “wet” cases, this air originates from a more moist (low-level) environment and is transported aloft, while in “dry” cases it originates from a drier (upper-level) environment, and is brought to lower altitude due to strong subsidence in the atmosphere above the boundary layer. A large-scale meteorological reanalysis from ECMWF (Fig. A3c and d) is also consistent with this interpretation, suggesting stronger subsidence and a corresponding increase in low-level divergence are present in the dry cases. The origin of low-level air as seen in the reanalysis showed no correlation with the wet/dry distinction.

The different characteristics of wet vs. dry cases are thus primarily attributable to differences in the large-scale advection which brings air masses to MCOH, as is evident in the CARDEX observations, the air mass back trajectories, and large-scale reanalysis. This difference in origin corresponds to greater variability in the clouds formed during “wet” conditions; by considering “dry” cases only, we can thus better analyze the subtle correlations present in each case. The variability within the dry cases is the focus of the following sections.

3 Characterization of observed high- vs. low-pollution conditions during CARDEX

Analysis of the meteorological conditions observed during CARDEX indicated that there was no correlation between cloud liquid water and any measured surface parameter for the CARDEX dataset as a whole. High variability is also present in the relationship between the measured cloud liquid water and surface aerosol concentration (Fig. 6a). However, when filtered by PWV into “wet” vs. “dry” cases, there is a statistically significant ($R = 0.42$ at the 95 % confidence level) increase in LWP (on a logarithmic scale) with increasing aerosol for the “dry” (PWV < 40 kg m⁻²) cases only (Fig. 6b). It is notable that this positive correlation is of opposite sign to the cloud burnoff effect, despite the presence of absorbing aerosol in the region, and is not indicative of a constant LWP as may be expected in a traditional analysis of the first indirect effect.

Figure 6 shows the cloud LWP increases with increasing aerosol concentration for “dry” cases only. In the following section we focus on these dry cases, which correspond to a well-defined, structured boundary layer as described above. In this analysis, we use all low/high pollution dry days (Table 1) where available (i.e. large-scale reanalysis and satellite observations); observations from the UAVs are necessarily limited to the subset of these days when a UAV was flown (Table 2). “Low pollution” cases are defined as having surface CPC measurements less than 1000 cm⁻³ (9 flights over 5 days), and “high pollution” cases are defined as having surface CPC greater than 1500 cm⁻³ (17 flights over 20 days). For simplicity, in the following sections these are referred to as Case L and Case H. The “moderately polluted” cases (1000 < CPC < 1500 cm⁻³) are excluded from the figures in order to bring focus to the high/low pollution contrast; however, Table 4 shows that these observations consistently fall between Case L and Case H, and in many cases they are in fact closer to Case H values.

Atmospheric aerosol effects in a trade cumulus regime

K. Pistone et al.

Title Page

Abstract

Introduction

Conclusions

References

Tables

Figures



Back

Close

Full Screen / Esc

Printer-friendly Version

Interactive Discussion



3.1 Surface and boundary layer characteristics

The UAV flight data offer valuable insights into the possible mechanisms behind the observed positive correlation between LWP and pollution. Figure 7 shows the observed Case L and Case H flight profiles from the aerosol-radiation UAV, while Fig. 8 shows the difference between the means of Case H and Case L. Note that Case H is uniformly more polluted (as measured by both the CPC and aethalometer) through the lower atmosphere up to about 2 km, at which point average pollution decreases for both cases. This is true for all cases except for one Case L flight which sampled an elevated aerosol plume. Case H exhibits warmer temperatures throughout the atmospheric column, with the maximum mean difference between the two cases occurring around the temperature inversion/cloud layer altitude (due to systematic differences in inversion height for Case L vs. H). The more polluted cases rather uniformly have higher boundary-layer relative humidity, and substantially higher free troposphere relative humidity. The slight negative values observed in the mean difference RH (H-L) (Fig. 8) around 800 m correspond to differences in the average altitude of the sub-cloud mixed layer between the two cases, which is higher in altitude for Case L. Case H again has higher RH above the inversion, which may partly facilitate the correspondingly larger average cloud water content in this case.

It is clear from these figures that higher pollution days are correlated with both higher water vapor content and higher temperatures in the entire atmospheric column, particularly around the temperature inversion ($\sim 800\text{--}1500\text{ m}$) which is itself stronger in Case H.

The summary of the mean values for each pollution case is illustrated in Fig. 9, and values are given in Table 4. The less polluted dry cases correspond to greater surface wind speed and lower surface specific and relative humidities (Fig. 10), although the total-column PWV did not show a statistically-significant difference. Perhaps most strikingly, Case H shows smaller surface latent heat flux when compared with Case L, indicating that the higher observed atmospheric humidity is not due to increased sur-

Atmospheric aerosol effects in a trade cumulus regime

K. Pistone et al.

Title Page

Abstract

Introduction

Conclusions

References

Tables

Figures



Back

Close

Full Screen / Esc

Printer-friendly Version

Interactive Discussion



Atmospheric aerosol effects in a trade cumulus regime

K. Pistone et al.

Title Page

Abstract

Introduction

Conclusions

References

Tables

Figures



Back

Close

Full Screen / Esc

Printer-friendly Version

Interactive Discussion



face evaporation. While this is in large part due to the lower observed wind speed in Case H, the lower surface fluxes observed during increased aerosol conditions may partially be a result of surface dimming due to increased atmospheric absorption by black carbon and other absorbing aerosols (Ramanathan and Carmichael, 2008; Stanhill and Cohen, 2001; Wild, 2009).

Figure 9 and Table 4 show that mean temperature measured directly at the surface was not statistically different between the two categories. This is not inconsistent with the aircraft observations, which show a smaller difference between the two cases near the surface compared with higher altitudes (Fig. 8). Frequency distributions of some significant parameters are shown in Fig. 10.

The vertical structure of the atmosphere, as measured or calculated from the flight data, is further described in Fig. A5. These profiles provide insight into the differences in thermodynamic structure of each case. The profiles of equivalent potential temperature show θ_e to be constant within the mixed layer, while the saturation equivalent potential temperature (dashed line) decreases with height to the LCL. The layer of saturation, indicated by values of θ_e equal to those of θ_e^* , is significantly greater in vertical extent for the high pollution cases (approximately 200 m thick), whereas the low pollution profiles barely reach saturation before the temperature inversion. Above this layer is a sharp increase in θ_e^* following the inversion, coincident with a sudden decrease in θ_e due to the sudden decrease in q at the top of the boundary layer. Note that the intersection of θ_e and θ_e^* is higher in altitude for Case L, corresponding to the higher z_{cb} . The increase in θ_e^* across the boundary layer top is much greater for Case L than Case H, indicating that the high pollution cases are less stably stratified. This, in addition to the greater latent potential energy of these moist parcels, may result in Case H clouds more frequently achieving convection up through the temperature inversion, resulting in thicker (and thus higher LWP) clouds. While it was not possible to directly measure cloud top heights during CARDEX, this interpretation is corroborated by a statistical analysis of cloud tops in the region from the CALIPSO satellite (Wilcox et al., 2014), which found higher cloud tops associated with higher pollution levels.

These multiple datasets paint a consistent picture of the systematic differences between low and high pollution cases both at the surface and throughout the atmospheric column. A more polluted atmosphere is observed to be simultaneously warmer, more humid, and more convectively unstable. Further examination of these conditions using an idealized calculation (described in Appendix A2) indicates that only changes in humidity (rather than changes in temperature) would be able to account for differences in cloud height of the magnitude of those observed between low and high pollution conditions.

3.2 Large-scale variability between low and high pollution cases

While thus far we have discussed aerosol as the surface particle number concentration measured at the MCOH observatory, in the following large-scale analysis we use the satellite-retrieved AOD as a metric of pollution level to allow for analysis on a larger scale.

3.2.1 Regional aerosol patterns

Figure 11 (top row) shows the difference in mean MODIS AOD over the CARDEX region for the average of case (H-L) days. That is, (H-L) is taken as the mean of all high pollution (dry) days minus the mean of all low pollution (dry) days during the CARDEX period (Table 1). From left to right, the top row panels show the difference between average AOD for the 3, 2, 1, and 0 days preceding high-pollution minus low-pollution conditions (as measured at MCOH). The average Case L and Case H AODs with overlaid 1000 hPa wind fields are shown in Fig. A7.

It is evident from this large-scale perspective that the pollution level classifications as determined by the conditions over MCOH are not necessarily representative of the region as a whole. Indeed, the MODIS AOD over the CARDEX region for the mean of all Case L days indicates lower aerosol at MCOH, but high aerosol concentrations elsewhere in the northern Indian Ocean (Fig. A7). This is particularly true over the

Atmospheric aerosol effects in a trade cumulus regime

K. Pistone et al.

Title Page

Abstract

Introduction

Conclusions

References

Tables

Figures



Back

Close

Full Screen / Esc

Printer-friendly Version

Interactive Discussion



Case L and Case H overlaid by the 1000 hPa winds are shown in Fig. A8. The bottom row of Fig. 11 will be discussed in Sect. 3.3.

The analysis of Fig. 11 suggests that regions of high temperature are coincident with higher aerosol. We further explore this relationship with Fig. 12, which shows the correlation between AOD and T over the region. For both pollution cases, Fig. 12 shows a region of statistically-significant correlation (95 % level, indicated by hatching) between AOD and T. These correlation coefficients were determined by calculating the correlation R for each latitude/longitude point using the relationship between all days in question (i.e. all H or all L days).

The region of high positive and significant correlation is present over much of the Arabian Sea (the low-level source region to MCOH). The AOD-T correlation is less strong in absolute magnitude for Case H, but is significant over a broader spatial extent, while Case L suggests a stronger correlation concentrated in a smaller region of the Arabian Sea. That is, in the so-called low pollution cases (as defined by conditions at MCOH), the high-pollution, high-temperature air mass remains concentrated to the north rather than spreading – and dispersing – southward towards MCOH. Indeed, the difference between regionally-averaged AOD for the two cases over the region is only 0.05, a factor of 2–3 smaller than the maximum H-L difference. The correlation weakens in both magnitude and area of significance between Day H-2 and Day H, which further suggests a dispersion of the polluted air mass in Case H. This is consistent with the above interpretation of Fig. 11.

The smaller region of significant negative correlation to the east of the subcontinent may be explained by low atmosphere/surface dimming due to an elevated aerosol plume; at higher altitudes, for example at 875 hPa ($z \approx 1250$ m), the AOD and temperature T_{875} show a strong positive correlation in this region. Elevated aerosol plumes are generally seen to approach MCOH from this direction, following the upper-level wind field, consistent with the findings of Höpner et al. (2015).

Atmospheric aerosol effects in a trade cumulus regime

K. Pistone et al.

Title Page

Abstract

Introduction

Conclusions

References

Tables

Figures



Back

Close

Full Screen / Esc

Printer-friendly Version

Interactive Discussion



3.3 Correlations between aerosol, cloud water content, and atmospheric humidity

Figures 6 through 10 have indicated that more polluted conditions correspond to systematically greater measured cloud liquid water and to greater boundary layer water vapor content. While not the only factor, increased water vapor may to a degree lead to increased cloud LWP. We explore this relationship through a calculation of the adiabatic cloud LWC (Appendix A2), and conclude that the observed increase in cloud LWP for increased pollution is primarily attributable to a lowering of the cloud base due to increased atmospheric humidity, rather than to changes in temperature. That cloud bases are lower for the more polluted case is further corroborated by the measured lidar cloud base heights (Fig. 10), which indicated lower average z_{cb} for highly polluted cases, and by the UAV flight data (Fig. 13), which indicated systematically lower cloud penetrations for high pollution cases. While this is not definitively an indication that the cloud bases themselves were lower, as the plane penetrated clouds at a variety of altitudes of undetermined distance above z_{cb} , it is nonetheless consistent with lower cloud bases in Case H. The atmospheric profiles of equivalent potential temperature (Fig. A5) additionally support this, indicating that under highly polluted conditions, rising air parcels reach saturation at a lower altitude and the atmosphere exhibits a thicker saturated layer compared with the low-pollution conditions, further supporting the conclusion that the atmosphere is more humid and cloud bases are lower for high pollution conditions.

The bottom row of Fig. 11 shows the mean (H-L) relative humidity for the larger region surrounding MCOH; the H and L means separately overlaid with winds are shown in Fig. A9. Again, there is a notable difference between Case H and Case L: the H-L indicates that Case H corresponds to an air mass of high RH approaching MCOH over the four days prior to the given event. However, in contrast to the in contrast to the top two rows, the region of highest RH difference is seen to lag the high AOD/high temperature region by roughly one day, and develops rather than disperses with time. That

Atmospheric aerosol effects in a trade cumulus regime

K. Pistone et al.

Title Page

Abstract

Introduction

Conclusions

References

Tables

Figures



Back

Close

Full Screen / Esc

Printer-friendly Version

Interactive Discussion



Atmospheric aerosol effects in a trade cumulus regime

K. Pistone et al.

Title Page

Abstract

Introduction

Conclusions

References

Tables

Figures



Back

Close

Full Screen / Esc

Printer-friendly Version

Interactive Discussion



is, the region of higher RH is seen to be relatively small at -3 days, and subsequently strengthens in magnitude and spatial extent, approximately coincident in location with the maximum AOD/temperature, in the time leading up to the day in question. This lagged intensification of RH over the 4 day period suggests that some effect within the polluted air mass may be acting to increase its moisture content even as the air mass disperses. This effect is not seen in higher-altitude RH fields.

The correlation between AOD and RH (Fig. 14) exhibits a similar high-low contrast to that observed in the correlations between aerosol and temperature (Fig. 12): Case H has a weaker correlation over a larger region, whereas Case L is concentrated in a smaller, more highly-correlated region. However, this relationship differs significantly from the temperature plots in that instead of dispersing in the 1–2 days prior to Case H, the correlation between AOD and RH is seen to strengthen during this period. The question then becomes: what may be causing this higher humidity condition to develop? We now explore some potential causal mechanisms.

Discussion of potential humidification mechanisms

While the present observations cannot determine for certain the causal mechanism behind the observed correlations, we have provided evidence of correlations between aerosol and humidity. We next briefly speculate on potential mechanisms by which aerosol may affect atmospheric humidity (and thus by extension cloud properties) and present these as avenues for further study.

We have previously eliminated sea surface evaporation and decreased cloud formation as the primary causes of the observed higher humidity, due to the flux and LWP measurements already described. We may additionally neglect precipitation in this case, as drizzle was not observed in these clouds even under low-pollution conditions. This leaves large-scale factors, local top-of-boundary-layer fluxes, or possible aerosol-induced effects as potential contributing factors to the observed higher relative humidity. To first assess the possible influence of large-scale meteorological conditions on humidity, we turn to the HYSPLIT back trajectories, which show the near-surface

Atmospheric aerosol effects in a trade cumulus regime

K. Pistone et al.

[Title Page](#)[Abstract](#)[Introduction](#)[Conclusions](#)[References](#)[Tables](#)[Figures](#)[Back](#)[Close](#)[Full Screen / Esc](#)[Printer-friendly Version](#)[Interactive Discussion](#)

flow originating from the north/northwest region, with the upper-level flow under high pollution conditions in particular originating primarily from over the subcontinent, consistent with the results shown in Sect. 2. Upper-level humidity also appears to increase with time for the high pollution cases even as the air is subsiding, possibly indicative of increased mixing from within the boundary layer. Low pollution conditions exhibit less extended back trajectories (i.e. lower wind speed above the boundary layer), but come from generally the same direction. We thus found no clear meteorological distinction between the two cases which might explain the difference between their boundary-layer conditions. While meteorological conditions may be a potential causal factor of the observed correlation between aerosol and cloud properties (e.g. Mauger and Norris, 2007, 2010), the present observations are not sufficient to definitively establish or discard this hypothesis. Further study of the large-scale context is necessary to more fully explore the potential meteorological influences on the low/high pollution distinction and on the aerosol–humidity relationship.

Via aircraft and surface measurements as well as reanalysis data, we found the atmosphere to be warmer under more polluted conditions. The strong correlation between aerosol and temperature indicates that BC warming is a likely cause of this increased temperature. Taking a large-scale view, we find that the high aerosol optical depth is correlated with a high temperature over the region as a whole and in particular in the location of the air mass approaching MCOH. Simple calculations (Appendix A2) indicate that the increase in RH was the only potential factor which could account for the magnitude of the observed greater polluted cloud LWP compared with low pollution conditions, due to a lowering of the LCL and thus the cloud base height. However, the single-point observations made over MCOH are alone insufficient to establish the causal mechanism behind the observed correlations. In addition to higher temperature under high pollution conditions, we find that there is substantially higher atmospheric RH under polluted conditions.

For both pollution cases, there is a region of statistically-significant correlation (95 % level) between both AOD and T (Fig. 12), and AOD and RH (Fig. 14). While the devel-

Atmospheric aerosol effects in a trade cumulus regime

K. Pistone et al.

[Title Page](#)[Abstract](#)[Introduction](#)[Conclusions](#)[References](#)[Tables](#)[Figures](#)[Back](#)[Close](#)[Full Screen / Esc](#)[Printer-friendly Version](#)[Interactive Discussion](#)

of two separate climatologies based on the water vapor characteristics of the vertical profile, which result in different populations of clouds forming under each. When the data are filtered according to this climatological separation to account for the large natural variability of high-vapor conditions, we observe a distinct positive correlation between the aerosol concentration and cloud liquid water. In describing the systematic differences between low and high pollution conditions both from station data and from a large-scale perspective, we observe highly polluted conditions to be systematically warmer and more humid. From in-situ aircraft observations, we observed the boundary layer height under polluted cases to be lower, resulting in a lower cloud base which is responsible for the greater cloud liquid water. The large-scale analysis indicates that polluted air masses exiting the subcontinent are also warmer, while high-humidity conditions develop along with the air mass as it ages.

The CARDEX results show that high-aerosol conditions (corresponding to a high concentration of absorbing aerosol) are consistently warmer, and also tend to be systematically wetter than less-polluted cases; while the higher temperatures may be attributable to aerosol heating of the air mass (e.g. Ramanathan et al., 2007), with the given observations we are unable to definitively determine a causal mechanism to the observed aerosol–humidity correlation. We have offered some brief discussion of possible mechanisms which may be at play, including aerosol-driven humidification (either by influencing the mesoscale circulation or stabilizing the boundary layer locally), or meteorological conditions coincident to the higher aerosol conditions. Understanding the consequences of aerosol–cloud interactions in this region requires an understanding of how variations in atmospheric conditions such as temperature and humidity may impact cloud dynamics and water content. Additionally, future research aiming at understanding aerosol–cloud interactions as a whole, and effects of aerosols influencing atmospheric dynamics specifically, should incorporate both local observations of the instantaneous vertical structure and motion of the atmosphere, as well as large-scale observations to understand the air mass history and the potential influence of meteorology on these effects.

Appendix A:

A1 Extended Methods

The microwave radiometer (MWR) used during CARDEX was on loan from the Department of Energy's Atmospheric Radiation Measurement (ARM) Climate Research Facility. As described in the instrument's documentation (Morris, 2006), the MWR passively collects microwave radiation at two wavelength bands centered at 23.8 and 31.4 GHz, chosen to correspond to predominantly water vapor and liquid water emission, respectively. MWR LWP values were flagged as cloud retrievals if they were more than 35 g m^{-2} above a 1000-point running mean, a value chosen to reflect the instrument noise level and retrieval uncertainty. Two or more consecutive cloud-flagged retrievals are collectively considered a "cloud event" (Fig. 3, inset). An absolute maximum of 130 g m^{-2} was imposed on the running mean to avoid obvious cloud retrievals skewing the background mean. These values were empirically determined to maximize the number of clouds identified while discounting spurious "cloud events" that were a product of noise in the instrument. To this end, "cloud events" are defined as having two or more consecutive cloud-flagged retrievals; all single-retrieval "events" were excluded from analysis.

The mini-micropulse lidar (MPL) retrievals consisted of vertically-resolved backscatter data at 30 m resolution above 250 m, collected at 0.1 Hz. The MPL was operated daily between 22 February and 30 March for as many hours as was permitted by ambient operating conditions. Completely continuous operation was not possible due to the sensitivity of the instrument to conditions of heat, direct sunlight, and ambient humidity, which required constant operator supervision. The instrument was also switched off around noon particularly as the equinox approached to avoid direct overhead solar glare into the instrument cavity. The MPL was successfully operated for four overnight periods, on 20 and 22–24 March, to fully characterize the diurnal cycle.

Individual UAV flights were classified as "wet" or "dry" by taking the average PWV for ± 2 h around the flight time. During CARDEX, the MAC4 aircraft had 12 flights during dry

**Atmospheric aerosol
effects in a trade
cumulus regime**

K. Pistone et al.

Title Page

Abstract

Introduction

Conclusions

References

Tables

Figures



Back

Close

Full Screen / Esc

Printer-friendly Version

Interactive Discussion



lifting condensation level by 200 m, consistent with observed differences in z_{LCL} . This compares with a change of approximately 5 m resulting from a temperature change only. Thus the LCL is primarily determined by changes in RH. Note that the calculated z_{LCL} is 200–300 m lower than the z_{cb} indicated by the MPL; as surface air parcels ascend towards the LCL, they will mix with drier, cooler surrounding air, a factor which will raise cloud base height but is not accounted for in this idealized calculation.

Using the above result, we take changing the cloud base height to be a proxy for the effect of changing atmospheric RH.

We explore the magnitude of each effect (changing temperature vs. changing relative humidity) on the resulting cloud by calculating adiabatic cloud LWP for clouds of varying thicknesses and heights using values observed in CARDEX (Fig. A6; Table A2). While trade cumulus in particular have been observed to be significantly (60–90%) subadiabatic (Curry and Webster, 1999; Warner, 1955), with subadiabaticity increasing with cloud thickness, a calculation of the adiabatic liquid water provides a useful metric to diagnose the relative magnitude of a given change on the cloud liquid water content.

Table A2 and Fig. A6 indicate the magnitude of each effect (i.e. independently varying the relative humidity and temperature observed in cases H and L) on the cloud liquid water content. Temperature is taken to be the measured mean values T_{L} and T_{H} as shown in Fig. A6. For RH, z_{LCL} is taken as a proxy for z_{cb} ; for this idealized experiment, the heights $z_{\text{LCL,L}}$ and $z_{\text{LCL,H}}$ are approximated at 800 and 600 m, a difference approximately equal to the observed $\Delta z_{\text{LCL,(H-L)}}$. In-cloud lapse rates are assumed to be constant at -5.5 K km^{-1} .

For a cloud of fixed thickness, lowering the cloud base z_{cb} along the same temperature profile and raising the cloud base temperature for a fixed z_{cb} have roughly the same effect on cloud LWP: an increase of 17 and 22 g m^{-2} , respectively. Both of these changes are effectively negligible given the much larger magnitude of the observed H-L LWP differences we seek to explain. We additionally note that a physical thickening of the cloud due to higher cloud tops would have a similar effect, although the magnitude is somewhat smaller: for a 500 m thick cloud with cloud base at 800 m, the LWP would

Atmospheric aerosol effects in a trade cumulus regime

K. Pistone et al.

Title Page

Abstract

Introduction

Conclusions

References

Tables

Figures



Back

Close

Full Screen / Esc

Printer-friendly Version

Interactive Discussion



be 484 gm^{-2} , for an increase of 306 gm^{-2} over the base case. However, the observations suggest that a lowering of the cloud base is at least a significant contributing factor to the cloud thickening (e.g. Figs. 10, 13, A5).

Thus for clouds of similar thickness, we find that the higher temperature or relative humidity alone cannot explain the higher observed cloud water contents of Case H. However, for a lowering of the cloud base while holding cloud top constant (i.e. thicker clouds), the adiabatic LWC is found to increase by 350 gm^{-2} . Accounting for average subadiabaticity, this difference is still $\sim 200 \text{ gm}^{-2}$.

Acknowledgements. The CARDEX field campaign was sponsored and funded by the National Science Foundation Grant ATM07-21142 and conducted by the Scripps Institution of Oceanography at the University of California at San Diego in collaboration with the Desert Research Institute, Stockholm University, Argonne National Laboratory, and the Max Planck Institute for Chemistry. V. Ramanathan is the principal investigator of CARDEX, E. Wilcox is the Co-PI and H. Nguyen was the field director who conducted the campaign with full support by the government of Maldives. Full details of the CARDEX campaign can be found in: http://www-ramanathan.ucsd.edu/files/CARDEX_prop_Jun_20.pdf. This study is Paper #3 from the CARDEX campaign.

References

- Augstein, E., Schmidt, H., and Ostapoff, F.: The Vertical Structure of the Atmospheric Planetary Boundary Layer in Undisturbed Trade Winds over the Atlantic Ocean, *Bound.-Lay. Meteorol.*, 6, 129–150, 1974. 29377
- Betts, A.: The physics and parameterization of moist atmospheric convection, chapter 4, in: *Trade Cumulus: Observations and Modeling*, edited by: Smith, R. K., NATO ASI Series C, vol. 505, Kluwer Academic Publishers, Dordrecht, 99–126, 498 pp., 1997. 29377
- Corrigan, C. E., Roberts, G. C., Ramana, M. V., Kim, D., and Ramanathan, V.: Capturing vertical profiles of aerosols and black carbon over the Indian Ocean using autonomous unmanned aerial vehicles, *Atmos. Chem. Phys.*, 8, 737–747, doi:10.5194/acp-8-737-2008, 2008. 29349, 29351

Atmospheric aerosol effects in a trade cumulus regime

K. Pistone et al.

Title Page

Abstract

Introduction

Conclusions

References

Tables

Figures



Back

Close

Full Screen / Esc

Printer-friendly Version

Interactive Discussion



- Curry, J. A. and Webster, P. J.: Thermodynamics of Atmospheres and Oceans, Academic Press, San Diego, 238–239, 1999. 29368
- French, J., Vali, G., and Kelly, R.: Observations of microphysics pertaining to the development of drizzle in warm, shallow cumulus clouds, Q. J. Roy. Meteor. Soc., 126, 415–443, doi:10.1256/smsqj.56303, 2000. 29377
- Garstang, M. and Betts, A.: Review of tropical boundary-layer and cumulus convection – structure, parameterization, and modeling, B. Am. Meteorol. Soc., 55, 1195–1205, doi:10.1175/1520-0477(1974)055<1195:AROTTB>2.0.CO;2, 1974. 29377
- Heymsfield, A. and McFarquhar, G.: Microphysics of INDOEX clean and polluted trade cumulus clouds, J. Geophys. Res.-Atmos., 106, 28653–28673, doi:10.1029/2000JD900776, 2001. 29349
- Höpner, F., Bender, F. A.-M., Ekman, A. M. L., Praveen, P. S., Bosch, C., Ogren, J. A., Andersson, A., Gustafsson, Ö., and Ramanathan, V.: Vertical profiles of optical and microphysical particle properties above the northern Indian Ocean during CARDEX 2012, Atmos. Chem. Phys. Discuss., 15, 3907–3953, doi:10.5194/acpd-15-3907-2015, 2015. 29360
- LaMontagne, R. and Telford, J.: Cloud top mixing in small cumuli, J. Atmos. Sci., 40, 2148–2156, doi:10.1175/1520-0469(1983)040<2148:CTMISC>2.0.CO;2, 1983. 29377
- Lawrence, M.: The relationship between relative humidity and the dewpoint temperature in moist air – a simple conversion and applications, B. Am. Meteorol. Soc., 86, 225–233, doi:10.1175/BAMS-86-2-225, 2005. 29367, 29375, 29376
- Lawrence, M. G. and Lelieveld, J.: Atmospheric pollutant outflow from southern Asia: a review, Atmos. Chem. Phys., 10, 11017–11096, doi:10.5194/acp-10-11017-2010, 2010. 29379
- MacPherson, J. and Isaac, G.: Turbulent Characteristics of Some Canadian Cumulus Clouds, J. Appl. Meteorol., 16, 81–90, doi:10.1175/1520-0450(1977)016<0081:TCOSCC>2.0.CO;2, 1977. 29377
- Malkus, J. S.: Marine Meteorology: On the structure of trade-wind air below cloud, Technical Report #40: Unpublished Manuscript 56-52, Woods Hole Oceanographic Institution, doi:10.1575/1912/5433, 1956. 29377
- Malkus, J. S.: Marine Meteorology: On the structure of the trade wind moist layer, Technical Report #42: Unpublished Manuscript 57-9, Woods Hole Oceanographic Institution, doi:10.1575/1912/5443, 1957. 29377

Atmospheric aerosol effects in a trade cumulus regime

K. Pistone et al.

Title Page

Abstract

Introduction

Conclusions

References

Tables

Figures



Back

Close

Full Screen / Esc

Printer-friendly Version

Interactive Discussion



Mauger, G. S. and Norris, J. R.: Meteorological bias in satellite estimates of aerosol–cloud relationships, *Geophys. Res. Lett.*, 34, L16824, doi:10.1029/2007GL029952, 2007. 29363, 29364

Mauger, G. S. and Norris, J. R.: Assessing the impact of meteorological history on subtropical cloud fraction, *J. Climate*, 23, 2926–2940, doi:10.1175/2010JCLI3272.1, 2010. 29363

Morris, V. R.: Microwave Radiometer Handbook, Atmospheric Radiation Measurement Climatic Research Facility, US Department of Energy, ARM TR-016, 2006. 29366

Ramana, M. V. and Ramanathan, V.: Abrupt transition from natural to anthropogenic aerosol radiative forcing: observations at the ABC-Maldives Climate Observatory, *J. Geophys. Res.-Atmos.*, 111, D20207, doi:10.1029/2006JD007063, 2006. 29350, 29351

Ramana, M. V., Ramanathan, V., Kim, D., Roberts, G. C., and Corrigan, C. E.: Albedo, atmospheric solar absorption and heating rate measurements with stacked UAVs, *Q. J. Roy. Meteor. Soc.*, 133, 1913–1931, doi:10.1002/qj.172, 2007. 29349, 29351

Ramanathan, V. and Carmichael, G.: Global and regional climate changes due to black carbon, *Nat. Geosci.*, 1, 221–227, doi:10.1038/ngeo156, 2008. 29357

Ramanathan, V., Crutzen, P., Lelieveld, J., Mitra, A., Althausen, D., Anderson, J., Andreae, M., Cantrell, W., Cass, G., Chung, C., Clarke, A., Coakley, J., Collins, W., Conant, W., Dulac, F., Heintzenberg, J., Heymsfield, A., Holben, B., Howell, S., Hudson, J., Jayaraman, A., Kiehl, J., Krishnamurti, T., Lubin, D., McFarquhar, G., Novakov, T., Ogren, J., Podgorny, I., Prather, K., Priestley, K., Prospero, J., Quinn, P., Rajeev, K., Rasch, P., Rupert, S., Sadourny, R., Satheesh, S., Shaw, G., Sheridan, P., and Valero, F.: Indian Ocean Experiment: an integrated analysis of the climate forcing and effects of the great Indo-Asian haze, *J. Geophys. Res.-Atmos.*, 106, 28371–28398, doi:10.1029/2001JD900133, 2001. 29349

Ramanathan, V., Ramana, M. V., Roberts, G., Kim, D., Corrigan, C., Chung, C., and Winker, D.: Warming trends in Asia amplified by brown cloud solar absorption, *Nature*, 448, 575–578, doi:10.1038/nature06019, 2007. 29349, 29351, 29359, 29364, 29365

Roberts, G. C., Ramana, M. V., Corrigan, C., Kim, D., and Ramanathan, V.: Simultaneous observations of aerosol–cloud–albedo interactions with three stacked unmanned aerial vehicles, *P. Natl. Acad. Sci. USA*, 105, 7370–7375, doi:10.1073/pnas.0710308105, 2008. 29349, 29351

Rodts, S., Duijnkerke, P., and Jonker, H.: Size distributions and dynamical properties of shallow cumulus clouds from aircraft observations and satellite data, *J. Atmos. Sci.*, 60, 1895–1912, doi:10.1175/1520-0469(2003)060<1895:SDADPO>2.0.CO;2, 2003. 29377

- Simpson, J. and Dennis, A. S.: Cumulus Clouds and their Modification, NOAA Technical Memorandum ERL OD-14, National Oceanic and Atmospheric Administration, 1972. 29377
- Stanhill, G., and Cohen, S.: Global dimming: a review of the evidence for a widespread and significant reduction in global radiation with discussion of its probable causes and possible agricultural consequences, *Agr. Forest Meteorol.*, 107, 255–278, doi:10.1016/S0168-1923(00)00241-0, 2001. 29357
- Thomas, R. M., Praveen, P., Wilcox, E. M., Pistone, K., Bender, F., and Ramanathan, V.: First UAV Measurements of Entrainment Layer Fluxes with Coupled Cloud Property Measurements, American Geophysical Union, American Geophysical Union, Fall Meeting 2012, abstract #A53G-0211, 2012. 29351
- Warner, J.: The water content of cumuliform cloud, *Tellus*, 7, 449–457, 1955. 29351, 29368, 29377
- Wilcox, E. M., Thomas, R. M., Praveen, P., Pistone, K., Bender, F., Feng, Y., and Ramanathan, V.: Shallow Cumulus Clouds Embedded in a Deep Regional Haze: Results from Indian Ocean CARDEX Experiment, American Meteorological Society, American Meteorological Society 94th Annual Meeting, Paper #239815, 2014. 29357
- Wild, M.: Global dimming and brightening: a review, *J. Geophys. Res.-Atmos.*, 114, D00D16, doi:10.1029/2008JD011470, 2009. 29357

Atmospheric aerosol effects in a trade cumulus regime

K. Pistone et al.

Title Page

Abstract

Introduction

Conclusions

References

Tables

Figures



Back

Close

Full Screen / Esc

Printer-friendly Version

Interactive Discussion



Atmospheric aerosol effects in a trade cumulus regime

K. Pistone et al.

Table 3. Average surface values, standard deviations, and 10th and 90th percentile ranges observed for wet vs. dry conditions during CARDEX. Note the highly non-normal distributions of many of these parameters. With the exception of LEF and cloud values, these are calculated from the minute-averaged values for which $PWV < 40 \text{ kg m}^{-2}$ or $PWV > 40 \text{ kg m}^{-2}$. LWP and cloud base height are the more meaningful averages over cloud events only; boundary layer height additionally follows this definition to illustrate the position of cloud relative to the boundary layer. Due to the low nighttime wind speeds, eddy covariance fluxes were unresolvable; thus the values of LEF below are for daytime (6 a.m.–6 p.m. MVT) only. The corresponding 24 h values are 74.8 ± 54.3 (6.0–137.3) and 67.6 ± 64.1 (3.4–133.7) W m^{-2} for dry and wet conditions, respectively. Lifting condensation level is calculated from the approximation given in Lawrence (2005).

	dry conditions ($PWV < 40 \text{ kg m}^{-2}$)			wet conditions ($PWV > 40 \text{ kg m}^{-2}$)		
	mean	1σ	10–90 %iles	mean	1σ	10–90 %iles
Number of cloud events	267			363		
Cloud LWP (g m^{-2})	147.0	105.3	96.3–187.2	204.2	271.4	79.9–435.2
PWV (kg m^{-2})	31.4	4.6	25.0–37.9	47.8	5.5	41.0–56.5
CPC (cm^{-3})	1360	352	789–1797	1218	338	778–1621
AOD ₅₀₀	0.48	0.17	0.26–0.66	0.43	0.23	0.20–0.73
Wind speed (m s^{-1})	2.2	1.2	0.8–4.0	1.6	0.9	0.6–2.8
Surface temperature ($^{\circ}\text{C}$)	28.6	1.0	27.4–30.1	28.8	1.1	27.5–30.4
Surface pressure (hPa)	1008.2	1.9	1005.6–1010.7	1009.4	1.5	1007.4–1011.6
Relative humidity (%)	75.6	5.3	68.5–82.3	77.9	4.8	71.7–84.2
Specific humidity (g kg^{-1})	18.5	1.3	16.3–20.1	19.2	0.9	18.1–20.1
Boundary layer height (m)	895	193	674–1109	841	163	637–1071
Cloud base height (m)	849	252	583–1208	804	371	462–1448
Lifting condensation level (m)	629	137	454–812	570	127	405–731
Latent energy flux (W m^{-2})	79.8	56.2	11.4–148.9	70.6	64.2	6.9–135.4

Title Page	
Abstract	Introduction
Conclusions	References
Tables	Figures
◀	▶
◀	▶
Back	Close
Full Screen / Esc	
Printer-friendly Version	
Interactive Discussion	



Atmospheric aerosol effects in a trade cumulus regime

K. Pistone et al.

Table 4. Average surface values for low, medium, and high pollution for dry conditions (cases L, M, and H respectively). The numbers in parentheses indicate one standard deviation of the minute-averaged values for which $PWV < 40 \text{ kg m}^{-2}$ and $CPC < 1000 \text{ cm}^{-3}$ (low pollution), $1000 < CPC < 1500 \text{ cm}^{-3}$ (medium pollution), or $CPC > 1500 \text{ cm}^{-3}$ (high pollution). Due to the non-normal distributions of many of these parameters, the 10th and 90th percentile ranges are additionally shown (second line). LWP and cloud base height are the averages over cloud events only, as is boundary layer height, to illustrate the position of cloud relative to the boundary layer. Lifting condensation level is calculated from the approximation given in Lawrence (2005). Nighttime eddy covariance fluxes were unresolvable due to low wind speeds; thus the values of LEF below are for daytime (6 a.m.–6 p.m. MVT) only. The corresponding 24 h values are 98.5 ± 63.4 (37.4–169.3), 70.4 ± 51.5 (5.2–127.8), and 61.0 ± 42.1 (3.3–113.1) W m^{-2} for cases L, M, and H, respectively.

	Case L low, dry	Case M med, dry	Case H high, dry
Number of cloud events	45	129	89
Cloud LWP (g m^{-2})	97.5 (19.7) 75.0–121.8	145 (22.3) 105.2–163.8	175 (29.2) 109.0–293.6
PWV (kg m^{-2})	29.4 (4.2) 23.5–34.5	31.9 (4.9) 25.4–38.9	31.2 (4.2) 26.0–37.0
CPC (cm^{-3})	767.7 (118.9) 596–944	1319.9 (136.9) 1138–1487	1673.9 (169.8) 1512–1926
AOD ₅₀₀	0.38 (0.28) 0.14–0.82	0.47 (0.13) 0.26–0.64	0.50 (0.06) 0.45–0.56
Wind speed (m s^{-1})	2.86 (1.20) 1.43–4.56	2.31 (1.31) 0.77–4.25	1.84 (1.01) 0.59–3.17
Surface temperature ($^{\circ}\text{C}$)	27.97 (0.88) 26.84–29.02	28.64 (0.89) 27.67–30.07	28.80 (1.00) 27.65–30.26
Surface pressure (hPa)	1006.5 (1.3) 1004.9–1008.4	1008.0 (1.8) 1005.4–1010.3	1009.0 (1.7) 1006.8–1011.3
Relative humidity (%)	69.7 (4.2) 63.0–76.7	76.4 (4.2) 70.4–81.2	77.4 (4.6) 71.3–83.5
Specific humidity (g kg^{-1})	16.4 (1.2) 15.1–18.3	18.7 (0.9) 17.6–19.8	19.1 (0.9) 17.9–20.3
Boundary layer height (m)	1270 (173) 1009–1460	912 (161) 667–1054	784 (84) 669–863
Cloud base height (m)	1159 (165) 882–1290	848 (268) 595–1288	820 (203) 590–1077
Lifting condensation level (m)	775 (139) 597–952	608 (110) 481–765	583 (122) 423–746
Latent energy flux (W m^{-2})	113.9 (66.4) 55.7–193.9	74.3 (54.4) 5.5–149.4	64.6 (40.6) 12.7–113.1



BY

CC

Atmospheric aerosol effects in a trade cumulus regime

K. Pistone et al.

Table A1. Trade cumulus cloud properties as measured in previous studies.

Study	cloud base	cloud top	cloud width	cloud lifetime	updraft velocity	LWC
Malkus (1956) ^a	705 m	1.2–1.8 km			3–6 cm s ⁻¹	
Malkus (1957) ^a	200–3000 m thick		100–2000 m		0.5–5 ms ⁻¹	
Warner (1955) ^b	0.8–1.4 km	2.6–3.3 km	> 600 m	> 30 min		0.4–1.4 g m ⁻³
Simpson and Dennis (1972) ^c	500 m	3 km	500 m	5–10 min	2–3 ms ⁻¹	1–3 g m ⁻³
Augstein et al. (1974) ^d	600 m	1.3–2 km				
Garstang and Betts (1974) ^e	950 m	2300 m				
MacPherson and Isaac (1977) ^f	1700 m	4400 m	3.2 km			
LaMontagne and Telford (1983) ^g	1700 m	2650 m				
Betts (1997) ^h	950 hPa	800 hPa				
French et al. (2000)	~ 900 m	2–2.9 km	1 km	~ 30 min	4 ms ⁻¹ (5–7 max)	0.5–2 g m ⁻³
Rodts et al. (2003)	500 m	2500 m	10 m–3 km			

^a Western Atlantic data, 1946 and 1953.^b Measured vertically-resolved LWC within a cloud. Column LWP may be derived through vertical integration, yielding values of 800–1400 g m⁻².^c Clouds are subadiabatic due to entrainment of outside air.^d ATEX (1969) experiment in the equatorial Atlantic.^e After Malkus (1956). Clouds are capped by an inversion.^f Terrestrial (Canadian) cumulus, including some towering cu. Peak *w* was seen in the downdrafts rather than updrafts.^g Terrestrial (South Dakota) cumulus, Aug 1978. Altitudes are reported as above MSL, which is 1200 m below ground level.^h For comparison, the heights in hPa correspond to roughly 500 and 1500 m.

Title Page

Abstract

Introduction

Conclusions

References

Tables

Figures



Back

Close

Full Screen / Esc

Printer-friendly Version

Interactive Discussion



Atmospheric aerosol effects in a trade cumulus regime

K. Pistone et al.

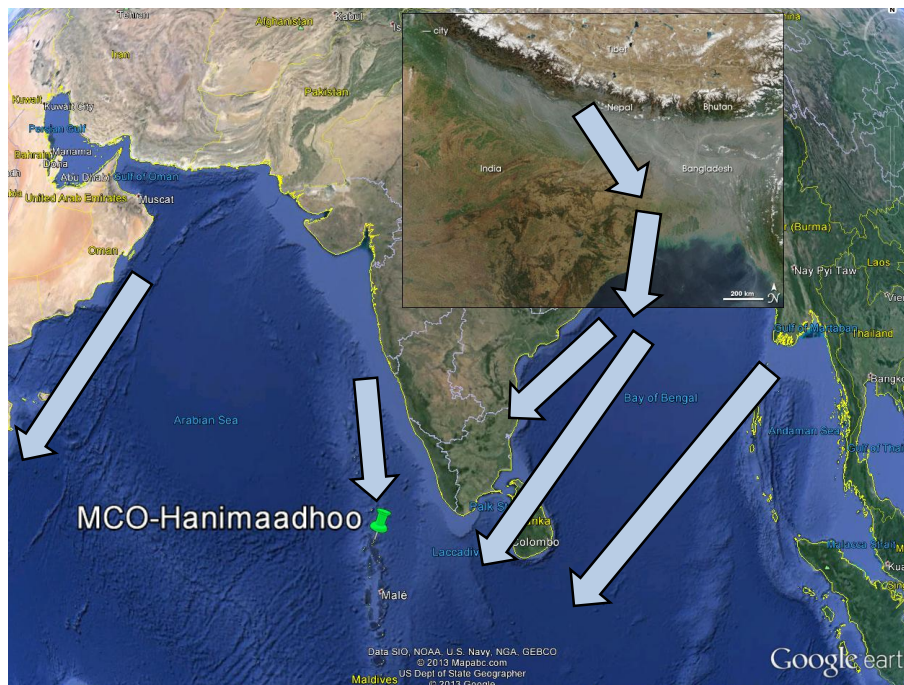


Figure 1. Map of the study location highlighting the Maldives Climate Observatory at Hani-maadhoo (MCOH). The overlay is a NASA MODIS satellite image of the region, showing an aerosol plume coming off the subcontinent. The presence of absorbing aerosols in the plume is evident from its greyish color. Predominant low-level flow during winter months (Lawrence and Lelieveld, 2010) is indicated by the arrows.

[Title Page](#)[Abstract](#)[Introduction](#)[Conclusions](#)[References](#)[Tables](#)[Figures](#)[◀](#)[▶](#)[◀](#)[▶](#)[Back](#)[Close](#)[Full Screen / Esc](#)[Printer-friendly Version](#)[Interactive Discussion](#)

Atmospheric aerosol effects in a trade cumulus regime

K. Pistone et al.

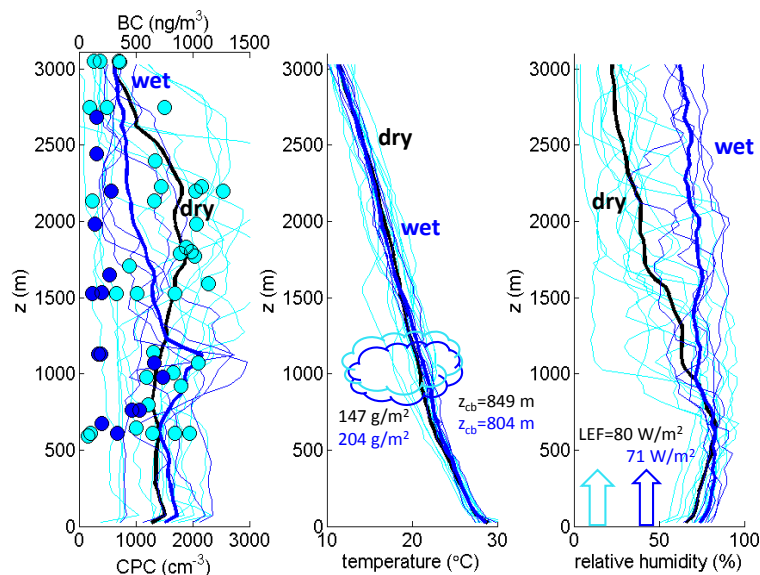


Figure 4. Aerosol, temperature, and relative humidity vertical profiles from the MAC4 aircraft for individual wet (dark blue) and dry (cyan) flights, as indicated by Table 2. The thin lines indicate individual profiles, and the thick lines indicate the ensemble mean. For clarity, the ensemble mean of the dry cases is shown in black. Black carbon retrievals are shown as discrete circles as they required a period of level flight to get an accurate reading. There were 12 dry and 5 wet flights with this aircraft; a description of the flight conditions and times may be found in Table 2. Note that the strong temperature inversion on dry days is most evident in the individual profiles rather than the means, as the latter tends to average out the inversion due to differing boundary layer heights. The average values of liquid water path (LWP), cloud base height (z_{cb}), and latent energy flux (LEF) are measured from the MWR, MPL, and gust probe instrumentation, respectively, at MCOH, and are also shown in Table 3.

Title Page

Abstract

Introduction

Conclusions

References

Tables

Figures

◀

▶

◀

▶

Back

Close

Full Screen / Esc

Printer-friendly Version

Interactive Discussion



Atmospheric aerosol effects in a trade cumulus regime

K. Pistone et al.

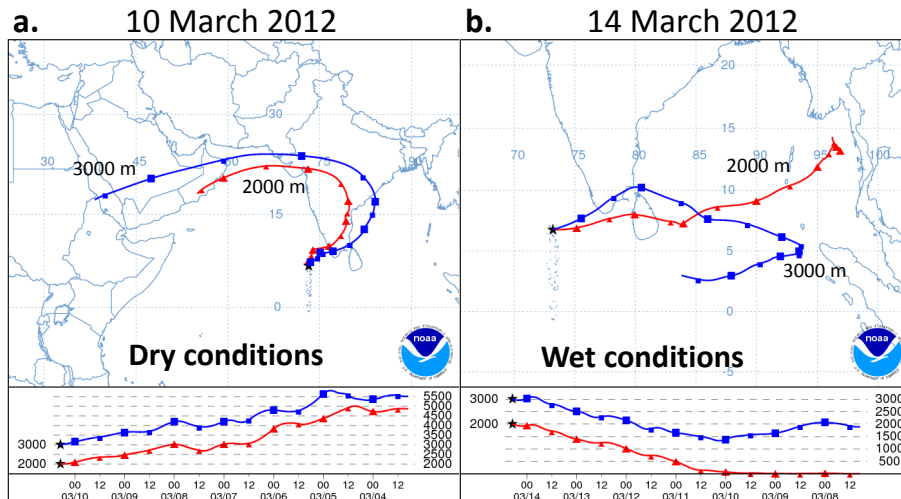


Figure 5. NOAA HYSPLIT 7-day back trajectories arriving at 07:00 Z (12:00 MVT) for **(a)** 10 March 2012, a typical “dry” day, and **(b)** 14 March 2012, a typical “wet” day. Visualization from the HYSPLIT-WEB tool (<http://ready.arl.noaa.gov/HYSPLIT.php>).

Title Page

Abstract

Introduction

Conclusions

References

Tables

Figures

⏪

⏩

◀

▶

Back

Close

Full Screen / Esc

Printer-friendly Version

Interactive Discussion



Atmospheric aerosol effects in a trade cumulus regime

K. Pistone et al.

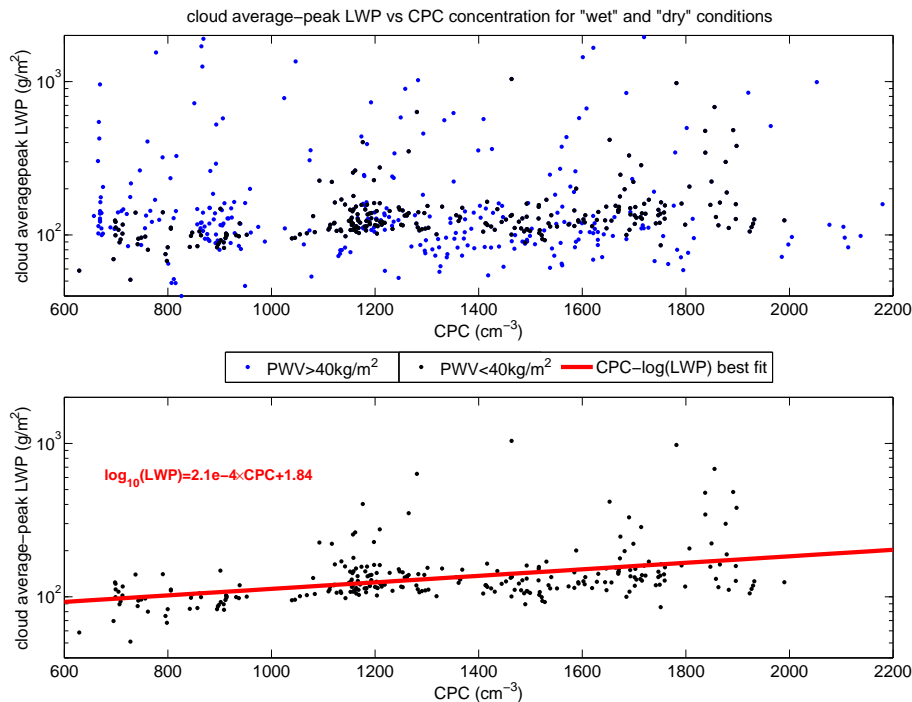


Figure 6. Cloud average-peak liquid water path vs. aerosol concentration, for all clouds (top; wet in blue, dry in black) and just dry condition clouds (bottom). Note the logarithmic scaling on the y axis. The red line indicates the linear best fit between CPC aerosol number concentration and $\log(\text{LWP})$.

Title Page

Abstract

Introduction

Conclusions

References

Tables

Figures



Back

Close

Full Screen / Esc

Printer-friendly Version

Interactive Discussion



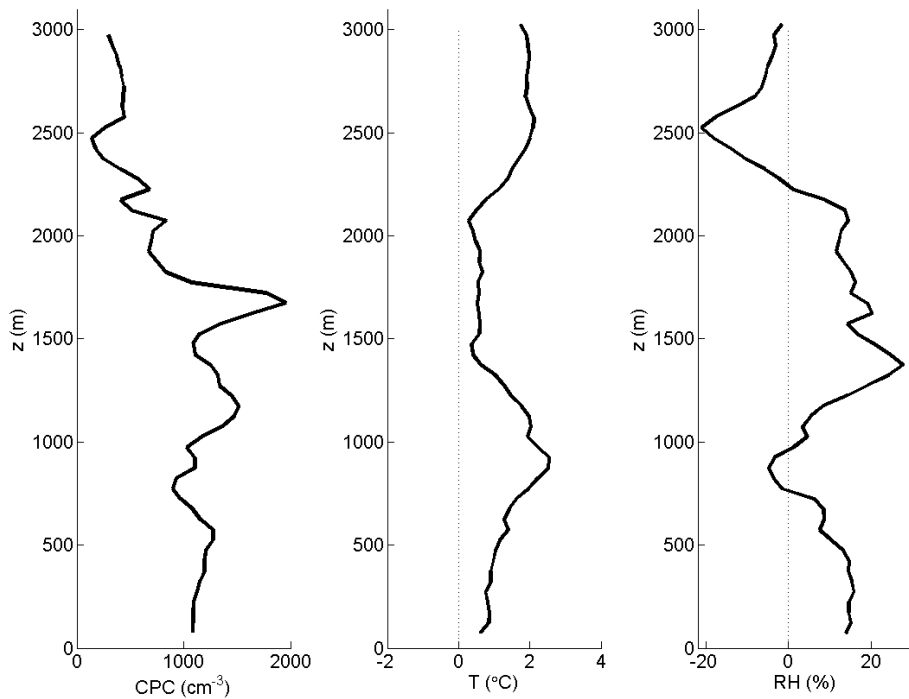


Figure 8. As in Fig. 7, here illustrating the H-L differences in measured MAC4 profiles of CPC, temperature, and relative humidity.

Atmospheric aerosol effects in a trade cumulus regime

K. Pistone et al.

Title Page	
Abstract	Introduction
Conclusions	References
Tables	Figures
◀	▶
◀	▶
Back	Close
Full Screen / Esc	
Printer-friendly Version	
Interactive Discussion	



Atmospheric aerosol effects in a trade cumulus regime

K. Pistone et al.

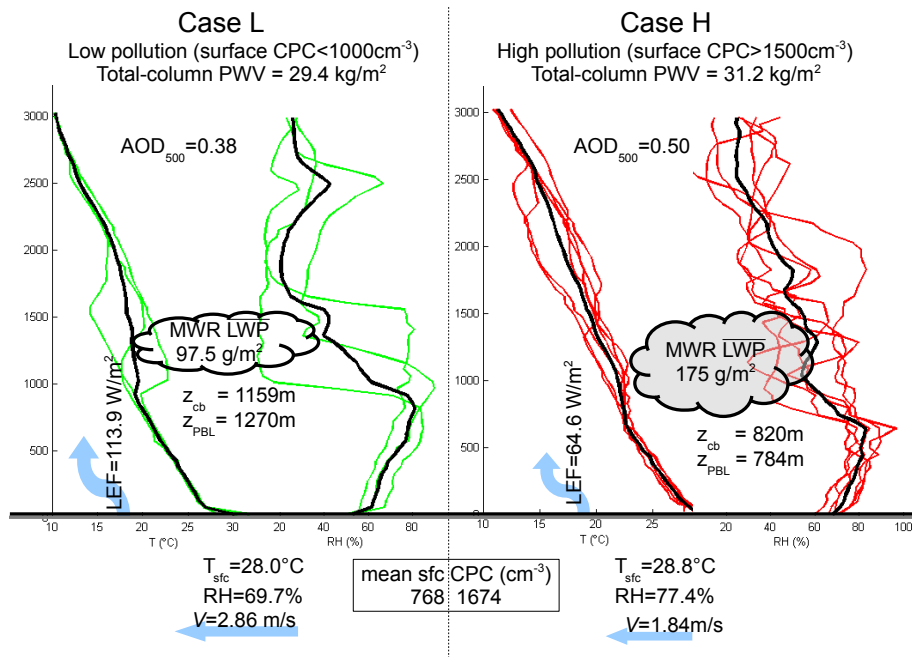


Figure 9. Characteristics of Case L vs. Case H conditions. By definition Case H has higher surface aerosol concentration; as expected, this is also true for AERONET-measured column AOD. Case H also sees higher humidity, lower surface vapor fluxes, and lower wind speed and, as shown by Fig. 6, has greater average cloud LWP. The lidar retrievals of cloud base and boundary layer height and the calculated LCL height are systematically lower for more polluted conditions.

Title Page

Abstract

Introduction

Conclusions

References

Tables

Figures



Back

Close

Full Screen / Esc

Printer-friendly Version

Interactive Discussion



Atmospheric aerosol effects in a trade cumulus regime

K. Pistone et al.

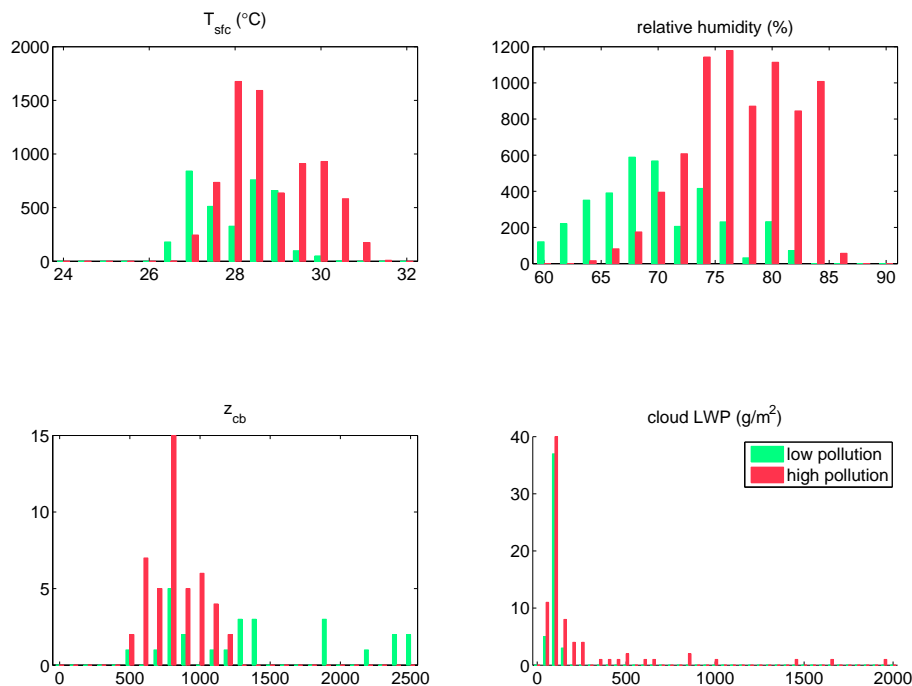


Figure 10. Frequency distributions of surface air temperature and relative humidity (minute data from MCOH), cloud base height (cloud-averaged data from MPL), and cloud liquid water path (cloud-averaged data from MWR) for low vs. high pollution cases.

[Title Page](#)[Abstract](#)[Introduction](#)[Conclusions](#)[References](#)[Tables](#)[Figures](#)[◀](#)[▶](#)[◀](#)[▶](#)[Back](#)[Close](#)[Full Screen / Esc](#)[Printer-friendly Version](#)[Interactive Discussion](#)

Atmospheric aerosol effects in a trade cumulus regime

K. Pistone et al.

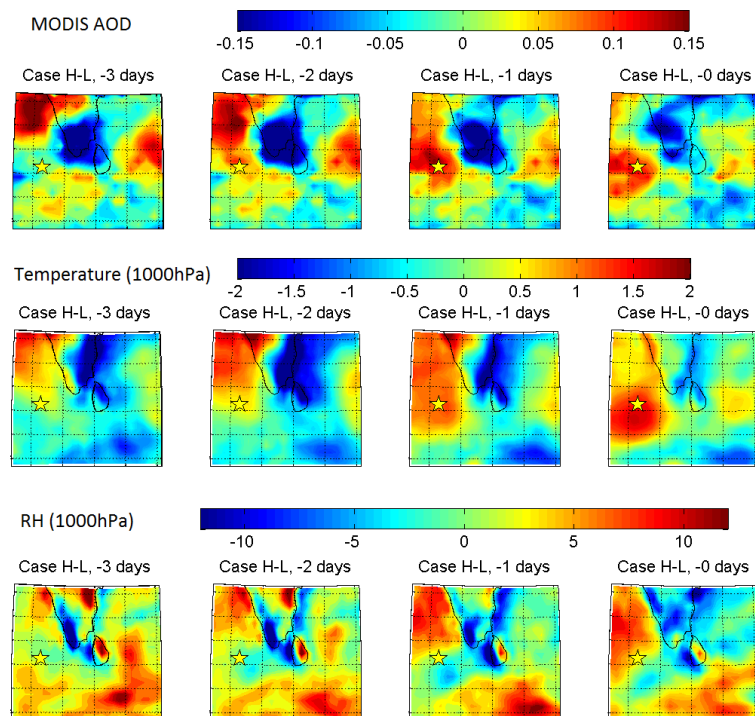


Figure 11. The difference in high minus low pollution conditions for MODIS AOD (top row) and ECMWF temperature (middle row) and relative humidity (bottom row) at 1000 hPa (approximately 75 m) for “dry” days as identified in Table 1. The 1-day lag between maximum AOD and temperature, and maximum relative humidity is evident in the day-to-day progression. Average Case L and Case H conditions overlaid with wind fields are shown in Figs. A7–A9.

[Title Page](#)[Abstract](#)[Introduction](#)[Conclusions](#)[References](#)[Tables](#)[Figures](#)[◀](#)[▶](#)[◀](#)[▶](#)[Back](#)[Close](#)[Full Screen / Esc](#)[Printer-friendly Version](#)[Interactive Discussion](#)

Atmospheric aerosol effects in a trade cumulus regime

K. Pistone et al.

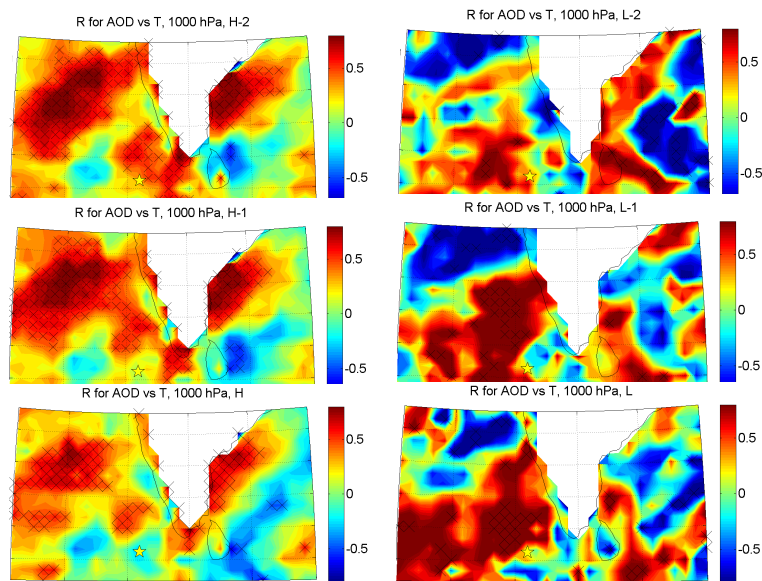


Figure 12. Correlation between AOD and 1000 hPa temperature for days leading up to high- (left) or low-pollution (right) events. The bottom row indicates the average of the days classified as a particular pollution event, while the middle and upper rows indicate the averages of one and two days prior, respectively. Hatching indicates a statistical significance at the 95 % level.

Title Page	
Abstract	Introduction
Conclusions	References
Tables	Figures
◀	▶
◀	▶
Back	Close
Full Screen / Esc	
Printer-friendly Version	
Interactive Discussion	



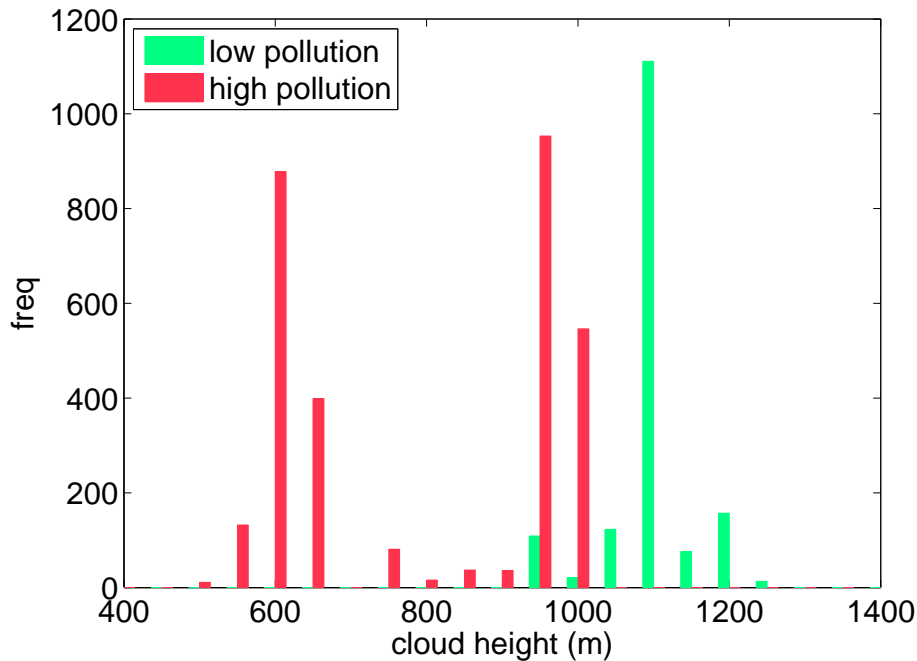


Figure 13. Altitude of cloud retrievals by MAC6 under low (green) and high (red) pollution cases, for 5 high-pollution and 2 low-pollution flights. Note that this figure shows the height at which the aircraft penetrated the clouds rather than cloud base or top height; however, the observations are consistent with overall lower cloud heights under polluted conditions.

Atmospheric aerosol effects in a trade cumulus regime

K. Pistone et al.

Title Page

Abstract Introduction

Conclusions References

Tables Figures

◀ ▶

◀ ▶

Back Close

Full Screen / Esc

Printer-friendly Version

Interactive Discussion



Atmospheric aerosol effects in a trade cumulus regime

K. Pistone et al.

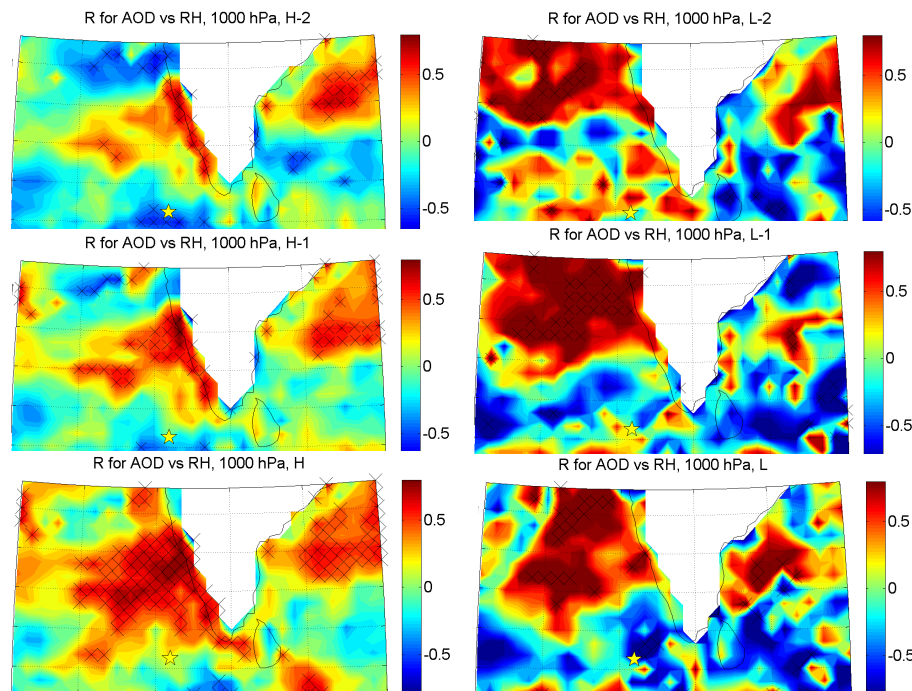


Figure 14. Correlation between MODIS AOD and ECMWF 1000 hPa relative humidity for days leading up to high- (left) or low-pollution (right) events. The bottom row indicates the average of the days classified as a particular pollution event, while the middle and upper rows indicate one and two days prior, respectively. Hatching indicates a statistical significance at the 95 % level.

[Title Page](#)[Abstract](#)[Introduction](#)[Conclusions](#)[References](#)[Tables](#)[Figures](#)[◀](#)[▶](#)[◀](#)[▶](#)[Back](#)[Close](#)[Full Screen / Esc](#)[Printer-friendly Version](#)[Interactive Discussion](#)

Atmospheric aerosol effects in a trade cumulus regime

K. Pistone et al.

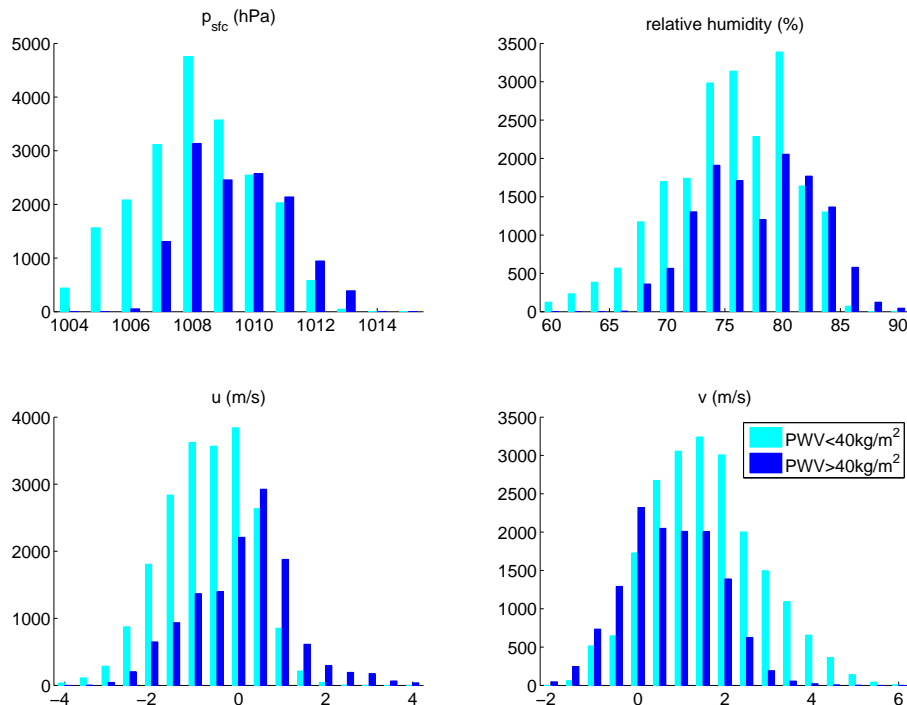


Figure A1. Distributions of MCOH variables on minute-resolution for low (PWV < 40 kg m⁻², cyan) and high (PWV > 40 kg m⁻², blue) water vapor conditions. Dry cases on average correspond to a lower surface pressure, lower surface humidity, and faster surface wind speed in both north/south (northerly) and east/west (westerly) directions.

Title Page

Abstract

Introduction

Conclusions

References

Tables

Figures



Back

Close

Full Screen / Esc

Printer-friendly Version

Interactive Discussion



Atmospheric aerosol effects in a trade cumulus regime

K. Pistone et al.

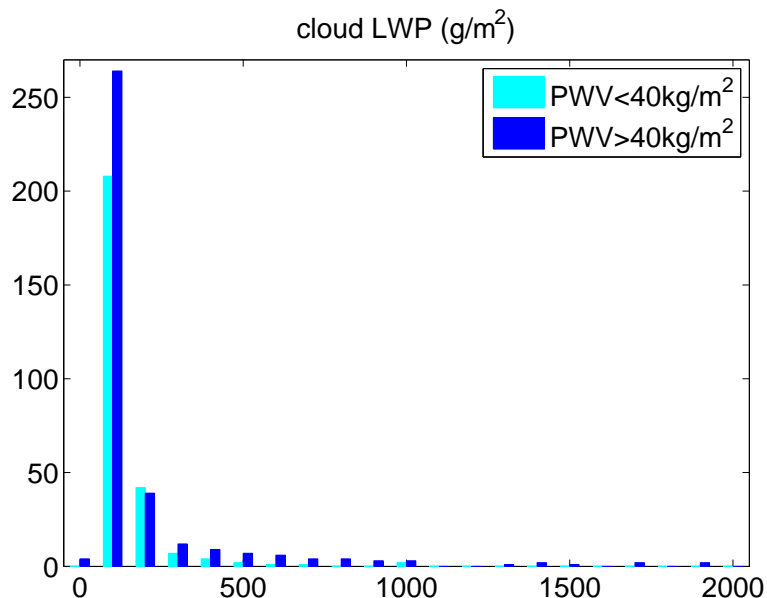


Figure A2. Frequency distribution of cloud LWP for wet (dark blue) and dry (cyan) cases. The clouds under the wet case exhibit more variability in water content than do clouds observed under dry conditions (Table 3), possibly due to a lack of a well-defined boundary layer topped by a temperature inversion, which would act to limit cloud vertical development as in the “dry” cases.

Atmospheric aerosol effects in a trade cumulus regime

K. Pistone et al.

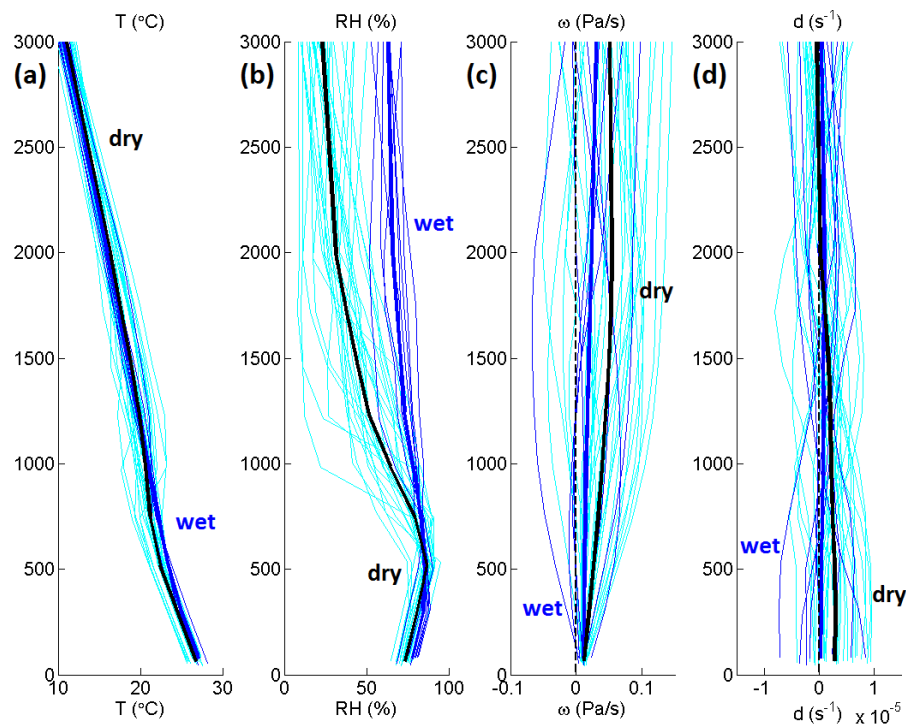


Figure A3. ECMWF temperature, relative humidity, pressure vertical velocity, and divergence over MCOH for wet (thin blue, mean in thick blue) vs. dry (thin cyan, mean in thick black) days during CARDEX. **(a)** and **(b)** exhibit good agreement with the observed vertical profiles measured by the aircraft: as in the flight data, the dry days exhibit a stronger temperature inversion and subsequent drop in humidity, whereas wet cases have consistently higher humidity above the 1000–1500 m inversion. Also consistent with the back trajectory analysis, there is stronger **(c)** subsidence and corresponding **(d)** divergence for the dry cases.

Atmospheric aerosol effects in a trade cumulus regime

K. Pistone et al.

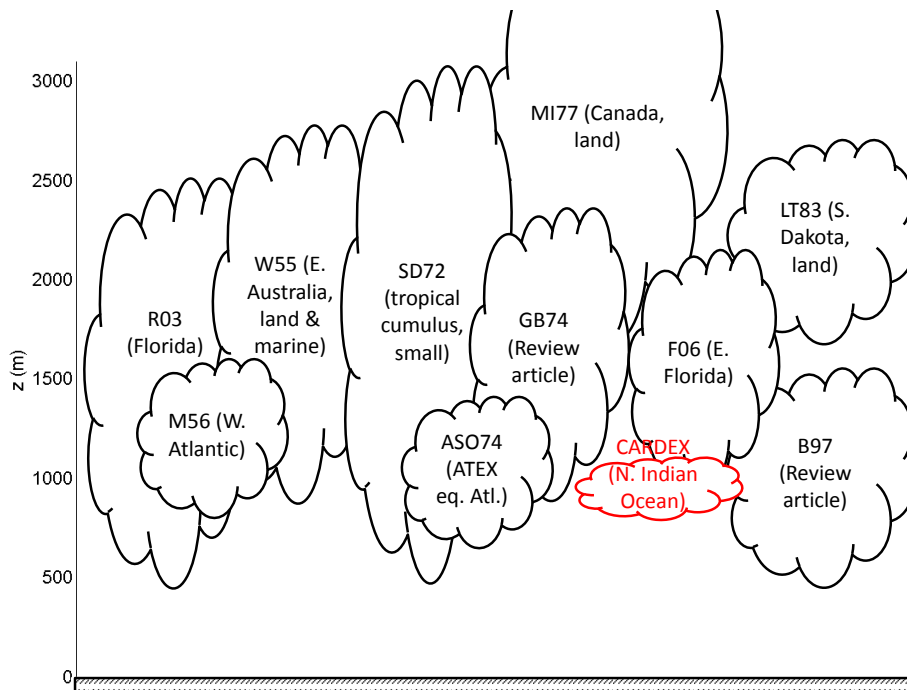


Figure A4. Previous descriptions of small cumulus according to the literature. Note that some clouds, especially those measured over land, are physically larger than the clouds observed in the Indian Ocean during CARDEX. References are those in Table A1.

Title Page

Abstract

Introduction

Conclusions

References

Tables

Figures



Back

Close

Full Screen / Esc

Printer-friendly Version

Interactive Discussion



Atmospheric aerosol effects in a trade cumulus regime

K. Pistone et al.

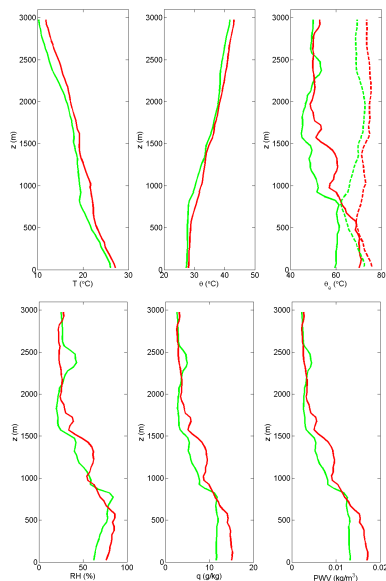


Figure A5. MAC4 vertical profiles for low (green) and high (red) pollution cases. The saturation equivalent potential temperature θ_e^* , is shown as dashed lines in the top right panel. Note that due to missing pressure data in two of the MAC4 flights, the calculated variables are determined using two less flights compared with Figs. 7 to 9. For consistency, these T and RH plots use the same data as in the calculated panels, and while the mean profiles are quantitatively slightly different, the high/low difference is essentially unchanged. Also of note is that the relative humidity increase with altitude between the surface and the top of the boundary layer appears to be primarily due to the change in temperature, as q remains fairly constant within this range. This is a product of the more strongly-defined boundary layer top with a sharp drop in RH for Case L. Whereas the RH of Case H decreases more slowly even for individual flights, the Case L average is higher than H just at the height of the Case L boundary layer top. This is less pronounced in q or PWV due to the coincident temperature inversion.

Title Page

Abstract

Introduction

Conclusions

References

Tables

Figures



Back

Close

Full Screen / Esc

Printer-friendly Version

Interactive Discussion



Atmospheric aerosol effects in a trade cumulus regime

K. Pistone et al.

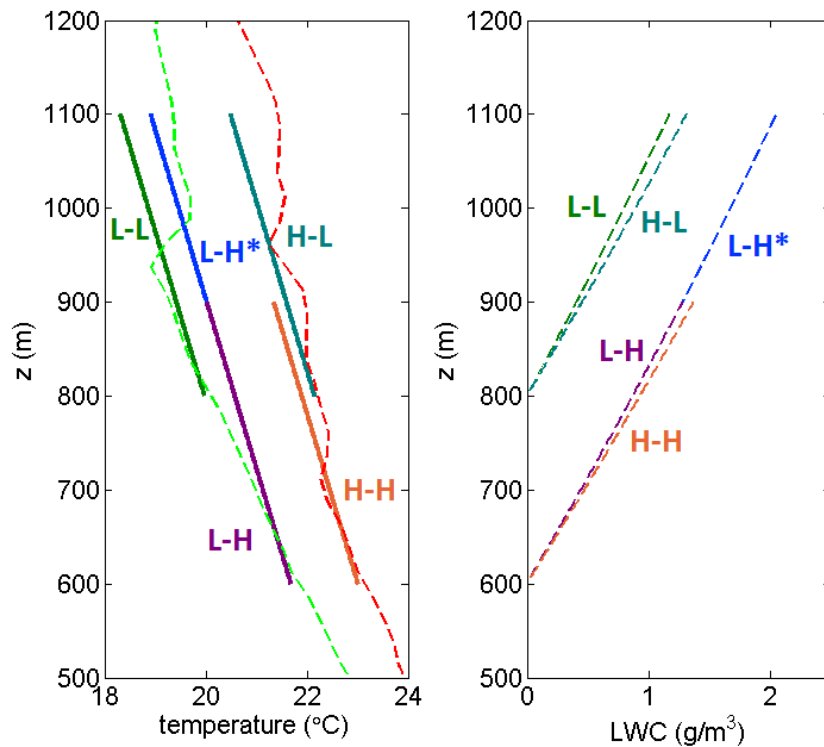


Figure A6. Adiabatic temperature profiles (left) and CLWC profiles (right) for the cases described in the text. Numerical values are given in Table A2.

Title Page	
Abstract	Introduction
Conclusions	References
Tables	Figures
◀	▶
◀	▶
Back	Close
Full Screen / Esc	
Printer-friendly Version	
Interactive Discussion	



Atmospheric aerosol effects in a trade cumulus regime

K. Pistone et al.

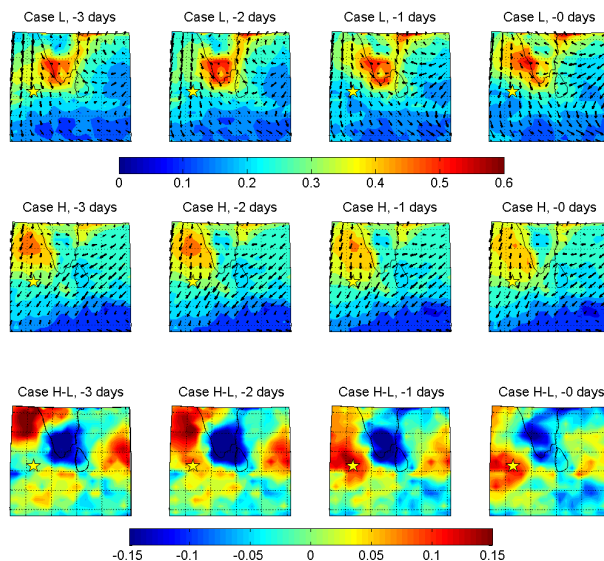


Figure A7. Average daily MODIS AOD for (top row) Case L, (middle row) Case H, and (bottom row) the difference between the two. Note that this includes all Case L and Case H days as identified in Table 1, rather than solely the ones on which a UAV was flown. The color scale shown is the same for both Case L and Case H, and the location of MCOH is indicated by the yellow star. From left to right, the columns are 0, 1, 2, or 3 days prior to a given classification. Note that while Case H corresponds to higher AOD over MCOH, Case L sees higher AOD over the Indian subcontinent. In Case H, the air mass of high aerosol concentration is seen to move south-southeastward to arrive over MCOH. This corresponds to the HYSPLIT and ECMWF low-level trajectories, indicating that upper-level pollution transport is not dominant in these cases. The arrows overlaid on the top two rows indicate the ECMWF average wind fields at 1000 hPa, showing similar north-northwesterly flow approaching MCOH in both cases. With increasing altitude, the wind can be seen to change to a northeasterly direction around the 850 hPa level, although this change occurs lower in altitude for Case H (~ 900 vs. ~ 800 hPa).

Title Page

Abstract

Introduction

Conclusions

References

Tables

Figures

◀

▶

◀

▶

Back

Close

Full Screen / Esc

Printer-friendly Version

Interactive Discussion



Atmospheric aerosol effects in a trade cumulus regime

K. Pistone et al.

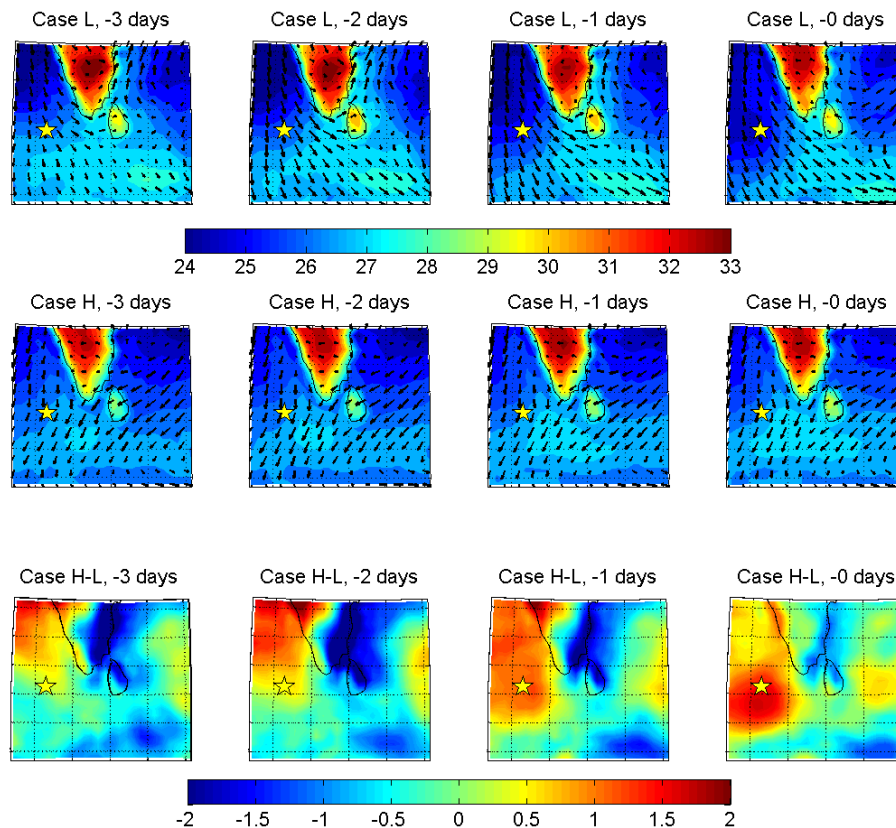


Figure A8. As in Fig. A7, but showing ECMWF 1000 hPa temperature (°C) for Case L, Case H, and the difference (H-L) for 3, 2, 1, and 0 days prior, overlaid with average winds.

[Title Page](#)[Abstract](#)[Introduction](#)[Conclusions](#)[References](#)[Tables](#)[Figures](#)[◀](#)[▶](#)[◀](#)[▶](#)[Back](#)[Close](#)[Full Screen / Esc](#)[Printer-friendly Version](#)[Interactive Discussion](#)

Atmospheric aerosol effects in a trade cumulus regime

K. Pistone et al.

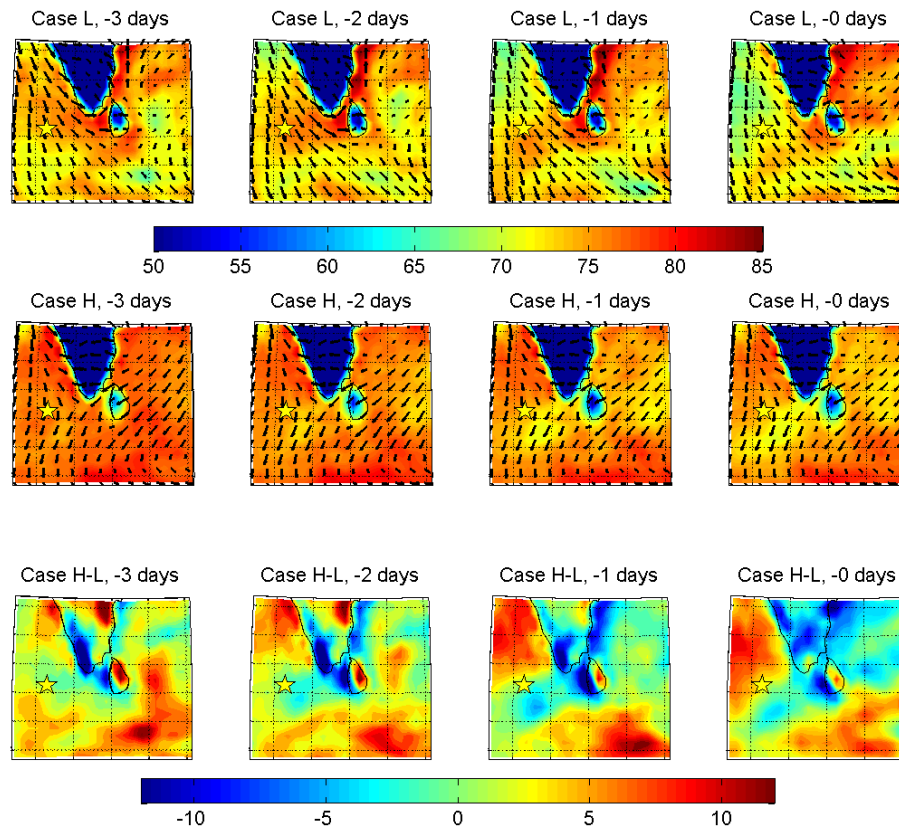


Figure A9. As in Figs. A7 and A8, but showing ECMWF 1000 hPa relative humidity (%) for Case L, Case H, and the difference (H-L) for 3, 2, 1, and 0 days prior, overlaid with average winds.

Title Page

Abstract

Introduction

Conclusions

References

Tables

Figures

◀

▶

◀

▶

Back

Close

Full Screen / Esc

Printer-friendly Version

Interactive Discussion



Atmospheric aerosol effects in a trade cumulus regime

K. Pistone et al.

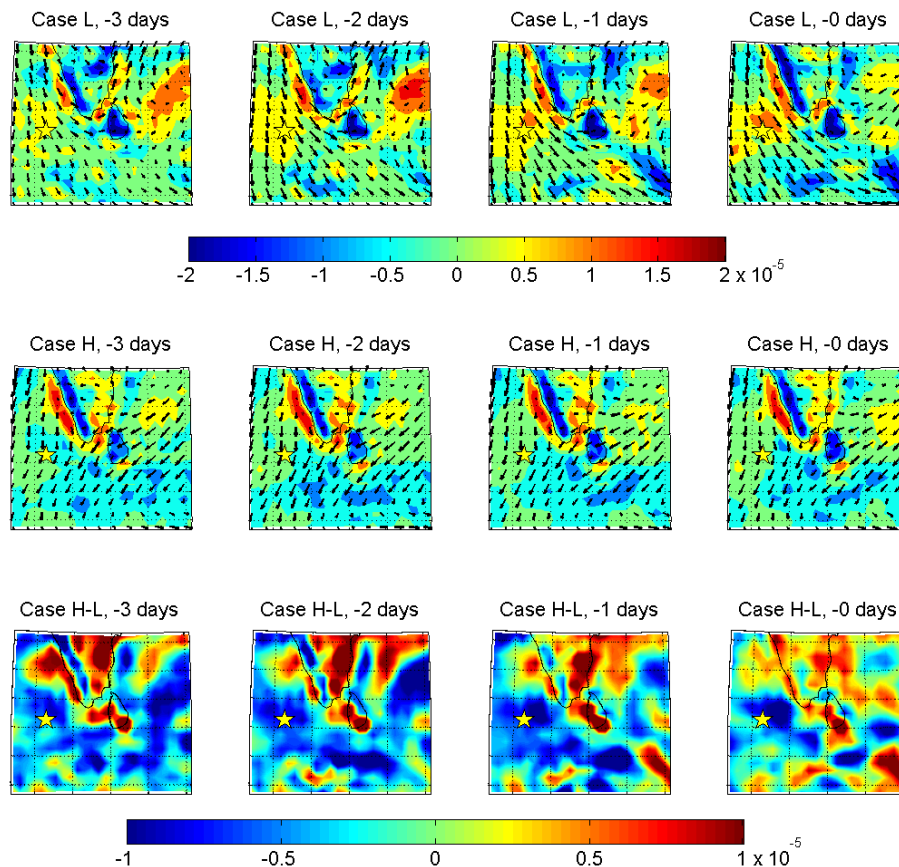


Figure A10. As in Figs. A7 through A9, showing ECMWF 1000 hPa divergence (s^{-1}) for Case L, Case H, and the difference (H-L) for 3, 2, 1, and 0 days prior, overlaid with average winds.

Title Page

Abstract Introduction

Conclusions References

Tables Figures

◀ ▶

◀ ▶

Back Close

Full Screen / Esc

Printer-friendly Version

Interactive Discussion

